ELSEVIER

Journal of Biomechanics 40 (2007) 3688–3699

JOURNAL OF BIOMECHANICS

www.elsevier.com/locate/jbiomech
www.JBiomech.com

Reliable simulations of the human proximal femur by high-order finite element analysis validated by experimental observations

Zohar Yosibash[a,*], Nir Trabelsi[a], Charles Milgrom[b]

[a]*Department of Mechanical Engineering, Ben-Gurion University of the Negev, Beer-Sheva 84105, Israel*
[b]*Department of Orthopaedics, Hadassah University Hospital, Jerusalem, Israel*

Accepted 5 June 2007

Abstract

Background: The mechanical response of patient-specific bone to various load conditions is of major clinical importance in orthopedics. Herein we enhance the methods presented in Yosibash et al. [2007. A CT-based high-order finite element analysis of the human proximal femur compared to in-vitro experiments. ASME Journal of Biomechanical Engineering 129(3), 297–309.] for the reliable simulations of the human proximal femur by high-order finite elements (FEs) and validate the simulations by experimental observations.

Method of approach: A fresh-frozen human femur was scanned by quantitative computed tomography (QCT) and thereafter loaded (in vitro experiments) by a quasi-static force of up to 1250 N. QCT scans were manipulated to generate a high-order FE bone model with distinct cortical and trabecular regions having inhomogeneous isotropic elastic properties with Young's modulus represented by continuous spatial functions. Sensitivity analyses were performed to quantify parameters that mostly influence the mechanical response. FE results were compared to displacements and strains measured in the experiments.

Results: Young moduli correlated to QCT Hounsfield Units by relations in Keyak and Falkinstein [2003. Comparison of in situ and in vitro CT scan-based finite element model predictions of proximal femoral fracture load. Medical Engineering and Physics 25, 781–787.] were found to provide predictions that match the experimental results closely. Excellent agreement was found for both the displacements and strains. The presented study demonstrates that *reliable and validated* high-order patient-specific FE simulations of human femurs based on QCT data are achievable for clinical computer-aided decision making.

Keywords: Proximal femur; Finite element analysis; p-FEM; Computed tomography; Bone biomechanics

1. Introduction

The mechanical response of an individual patient's bone, and the proximal femur in particular, is of major clinical importance for orthopaedists. Simulation of an individual's bone response to loads is nowadays limited because of difficulties in acquisition of bone's exact complex geometry and its anisotropic and inhomogeneous material properties which vary among individuals.

In the past three decades, three-dimensional finite element (FE) analyses were performed for predicting bone's mechanical response (see Keyak et al., 1990; Viceconti et al., 1998; Taddei et al., 2006, and references therein). FE methods are attractive because at the macro level the bone exhibits elastic linear behavior for loads in the normal range of regular daily activities Keaveny et al. (1994). Bone's geometrical representation may be easily obtained from Quantitative computed tomography (QCT) scans (Keyak et al., 1990; Lotz et al., 1991a; Couteau et al., 2000; Viceconti et al., 2004; Bessho et al., 2007) and structure-based models were shown to be appropriate when surface strains are of interest (Viceconti et al., 1998; Couteau et al., 2000; Taddei et al., 2007). The determination of bone's inhomogeneous mechanical properties and their assignment to the FE mesh is yet a major unsolved problem. The proximal femur consists of cortical (compact) and trabecular (cellular) regions. Homogenized

*Corresponding author. Tel.: +972 8 6477103; fax: +972 8 6477101.
E-mail address: zohary@bgu.ac.il (Z. Yosibash).

0021-9290/$ - see front matter © 2007 Elsevier Ltd. All rights reserved.
doi:10.1016/j.jbiomech.2007.06.017

mechanical properties of both regions as well as isotropic Young's modulus E were experimentally associated with bone apparent density (ρ_{app}) or bone ash density (ρ_{ash}) (Lotz et al., 1990, 1991b; Keaveny et al., 1994; Keller, 1994; Wirtz et al., 2000). Bone's density in turn can be correlated to QCT Hausfeld Units (HUs) resulting in E(HU) relationship (see e.g. Keller, 1994; Keyak and Falkinstein, 2003). The complexity in determining material properties is enhanced by the anisotropic response which is distributed inhomogeneously throughout the bone. The various material properties cannot be obtained from a scalar value (the HU) in QCT scans, so simplifications have to be applied. For example, an FE study (Peng et al., 2006) compared the response of the femur when isotropic or orthotropic material properties were assigned under two loading conditions (double-leg standing and single-leg standing) showing that differences between the two material property assignments are small.

In previous FE studies conventional h-version FE methods (h-FEMs) were applied in most of which the inhomogeneous distribution of material properties was attained by assigning constant distinct values to distinct elements (see, e.g. Taddei et al., 2007 and references therein), thus the material properties became mesh dependent. Furthermore, the bone's surfaces were approximated by piecewise flat tesselation or piecewise parabolic tesselation, which introduced slight un-smoothness of the surface, therefore limited the possibility to obtain accurate strain measures on bone's surface. For example, the recent study of Bessho et al. (2007) uses a semi-automatic tetrahedral mesh generation combined with shell elements on the peripheral surface for the FE analysis of many proximal femurs, mainly to assess their strength to fracture but not for the mechanical response (although good load to deflection response is mentioned). Some studies do show good experimental correlation between h-FEM's results and fracture load, but to the best of our knowledge, only three studies investigated quantitatively the differences between computed strains and displacements, and these measured experimentally on a femur bone (Lotz et al., 1991a; Keyak et al., 1993; Taddei et al., 2007; Yosibash et al., 2007). Only partial agreement is found, suggesting the need for better simulations.

In a recent work by the authors Yosibash et al. (2007) the p-version FE (p-FE) method was suggested for the simulation of the proximal femur mechanical response. p-FEMs have many advantages over conventional h-FEMs: accurate surface representation, faster numerical convergence rates achieved by increasing the polynomial degree p of the shape functions over the same mesh thus controlling numerical errors easily. Also, the inhomogeneous Young's modulus can be described as a spatial inhomogeneous function within the model, and elements may have large aspect ratios (required in cortical regions being thin and long) and may be strongly distorted (Szabó and Babuška, 1991). In Yosibash et al. (2007) p-FEM results for a human fresh-frozen proximal femur model were compared to a corresponding experiment showing good correlation for displacements and partial correlation for the strains. The p-FE structure-based model was created from QCT data having an internal surface separating trabecular and cortical regions. An isotropic inhomogeneous material model was adopted for which Young's modulus was determined as follows: First, in the cortical and trabecular regions HUs were recalculated in each voxel using a moving average (Kenney and Keeping, 1962) (see simplified concept in Taddei et al., 2004). Next the spatial representation of the apparent density (ρ_{app}) was determined by least-mean square methods (LMS). Finally Young modulus was represented as a smooth function by an $E(\rho_{app})$ connection according to Cody et al. (2000), independent of the mesh.

Because of the unsatisfactory simulation results for the strains, and following the experience gained in our previous work, herein a new and improved model creation and experimental procedure are followed on another human fresh-frozen bone. A new loading machine with better measuring devices was used, a larger number of strain gauges were bonded on the bone's surface, horizontal displacement of femur's head was recorded, and finally two different configurations of load application (a flat plate in addition to a cone) were considered. A new method for the generation of bone's surfaces from QCT data was employed (smoothing algorithms were used with fewer patches) and hexahedral meshes were also created. We also reinvestigated the influence of E(HU) relations on the results and performed many sensitivity studies of the FE models. The new methods resulted in an excellent correlation (for both displacements and strains) for the p-FE results and in vitro experimental observations. The results in Yosibash et al. (2007) were reanalyzed according to the newly presented methods showing a considerably better agreement with experiments.

2. Methods

A fresh-frozen femur of a 21 year-old female donor was deep-frozen shortly after death (caused by a stroke). The bone was determined to be free of skeletal diseases by inspecting the general medical history of the donor, taking X-ray images to ensure that no bony lesions were present and taking bacterial and viral cultures. After defrosting, soft tissue was removed from the bone by a combination of sharp and blunt dissection. The bone was degreased with ethanol, and at sites with minimal curvature on which strain gauges (SGs) were to be applied the bone was roughened with 400 grit sandpaper and again cleaned with ethanol. Strain gauges were serially bonded to the bone using M-Bond 200 Cyanoacrylate Adhesive (Measurements Group, Inc., Raleigh, NC, USA).

The proximal femur was cut and affixed with six bolts to a cylindrical sleeve and fixed by PMMA. Thereafter QCT scans were performed on a Phillips Brilliance 16 CT (Eindhoven, Netherlands) with following parameters: 140 kVp, 250 mAs, 1.5 mm slice thickness, axial scan without overlap, with pixel size of 0.73 mm (512 pixels covering 373 mm field size). Mechanical experiments started following the QCT scans, 8 h after bone mounting and lasted for 36 h. During the bone preparation and between tests it was hydrated and stored in a cold humid container and in refrigeration overnight. Following the in vitro experiments a p-FE model was generated based on QCT scans and simulations performed to mimic

the experiments, after which the FE results were compared to the experimental observations for validation purposes.

2.1. In vitro experiments

In vitro experiments on the fresh-frozen proximal femur were performed to assess the validity of FE simulations. The experimental system includes a mounting jig, loading and measurement equipment and data acquisition equipment. The bone was loaded by a load controlled machine (Instron 5500R). The bone mounting jig is documented in Yosibash et al. (2007) allowing bone clamping at several discrete inclination angles. A ball and socket joint with a steel ball between two brass cones was used to prevent moments on the loading arm (Fig. 2). Two Solartron DFg5 Direct Current Linear Variable Displacement Transducers (DC-LVDT) measured the femur head vertical and horizontal displacements. They were positioned on stand arms with their core placed on femur's head (Fig. 1, right, Fig. 2).

Eight uni-axial SGs (Vishay CEA-06-062UR-350) with 1.6 mm active length and 350 Ω resistance were installed on the surface of the proximal

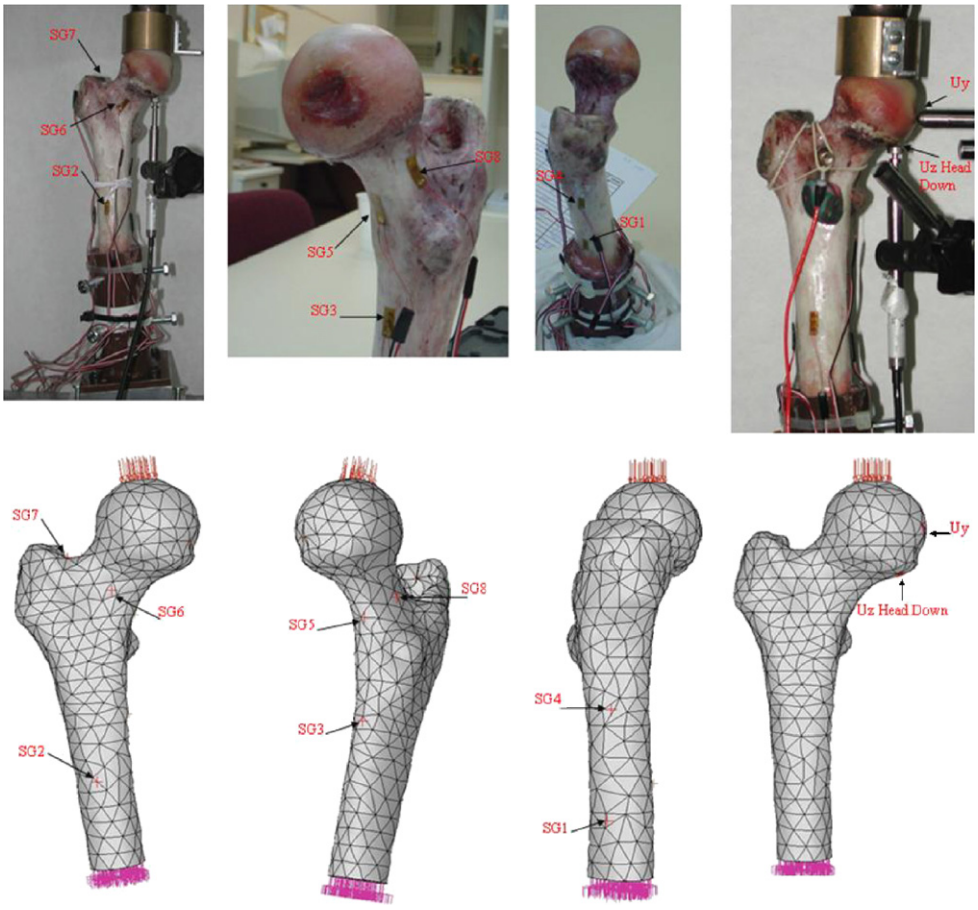

Fig. 1. Locations at which displacements and strains were measured.

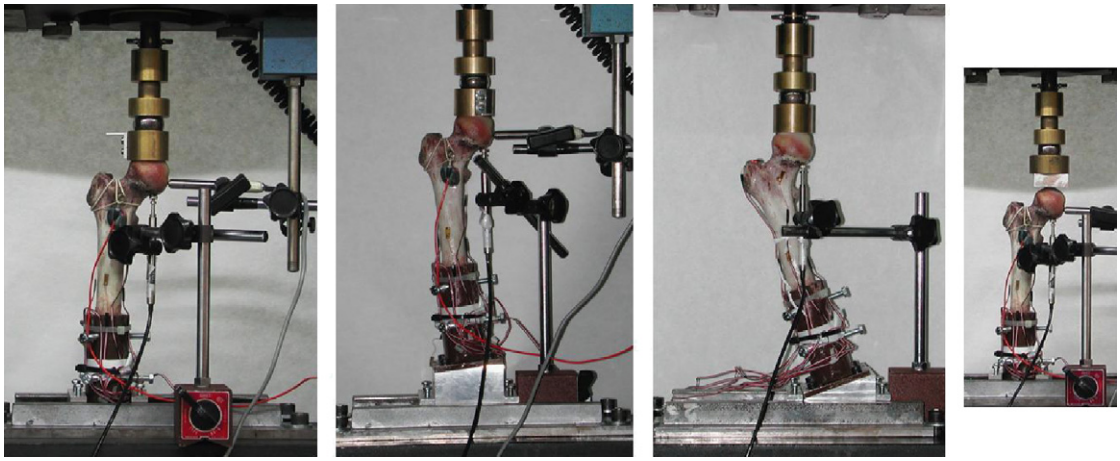

Fig. 2. Experiments on fresh-frozen bone at different inclination angles (from left to right): 0° ,7°, 20°, 0°-flat plate loading.

femur at the inferior and superior parts of the femur neck and on the medial and lateral femur shaft (Fig. 1). SGs, machine load–cell and the two LVDT outputs were recorded and processed after the experiments completion. Forces of up to 1250 N were applied (corresponding to more than half an average body weight but smaller compared to bone's linear response regime). These simulate a simple stance position configuration in which the femur is loaded through its head while the femur is inclined at $\approx 7^\circ$ to the shaft axis Jensen (1978) (along a virtual line that connects the femur head to the middle cavity in the femur diaphysis (intercondylar fossa)). Three inclination angles were considered: 0° for maximal sensitivity, 7° as in the natural stance posture, and 20° as in Keyak et al. (1993). At each inclination angle three or four consecutive monotonically loading–unloading patterns at a slow displacement rate of 0.5 mm/min were followed: Load to 500 N, release; load to 750 N, release; load to 1000 N, release; and finally load to 1250 N, release.

Fig. 3. The three regions of the proximal femur model. The trabecular region was divided into two sub-regions, each with a different spatial field for Young's modulus.

2.2. Proximal femur's geometric representation and p-FE mesh generation

The FE mesh of the proximal femur is constructed from the QCT along the steps detailed in Yosibash et al. (2007). Herein improvements compared to that work are emphasized. All DICoM (Digital Imaging and Communication in Medicine) format QCT scans were *automatically* manipulated by Matlab programs. First the scans are transformed into binary images in which non-zero pixels belong to the bone and the value 0 is assigned to pixels representing the background. The proximal femur bone's axis is aligned with the z-axis, so that it occupies the length $0<z<155.5$ mm. No exact HU exists that distinguishes between the cortical and trabecular regions, although bone having $\rho_{app}<0.7\,g/cm^3$ is often regarded as trabecular, and having $\rho_{app}>1.2\,g/cm^3$ is regarded as cortical (Cowin and Ashby, 2001). In Alho et al. (1988), Esses et al. (1989), Heismann et al. (2003), Bayraktar et al. (2004) the trabecular bone is associated with $HU<200-500$ and $\rho_{app}<0.75-0.97\,g/cm^3$. We associated voxel values of $HU>700$ with the cortical bone and values of $HU\leqslant 700$ to the trabecular bone, and accordingly QCT slices are divided into three main groups: cortical only ($0<z<78$ mm), trabecular and cortical ($78<z<115.5$ mm) and mostly trabecular ($z>115.5$). Exterior, interface and interior boundaries are traced and x–y arrays are generated, each representing different boundaries of a given slice (see first two left pictures in Fig. 4 for the intermediate and outer boundary detection). These arrays are manipulated by a 3D smoothing algorithm that generates smooth raw data arrays by a 3D spherical filter, 2D averaging filter and spline interpolation (3D spherical filter calculates the new location of each point in a specific slice using data from other slices around it). The smooth edges, using cubic spline interpolation, are saved as new arrays in a different text file that is read into the CAD package SolidWorks-2006 (SolidWorks Corporation, MA, USA). All text files are used to generate smooth closed splines, after which the surfaces are created by the "Loft" function and solid bodies generated. It is important to note that large surfaces are generated, in contrast with many small patches as in Yosibash et al. (2007). Four different solid parts are then created: entire bone, cavity region,

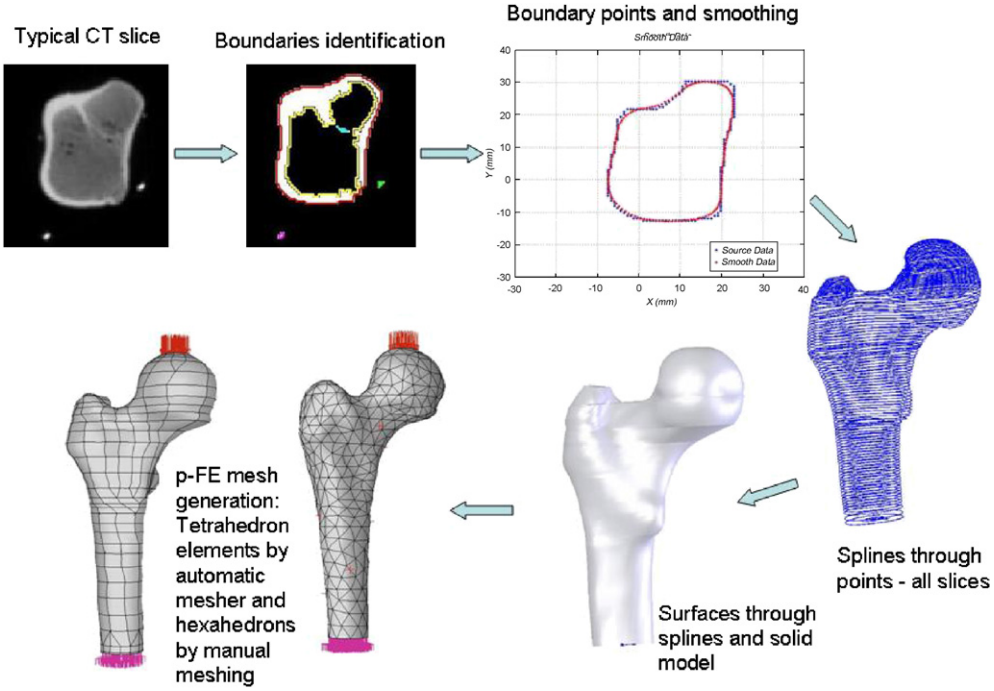

Fig. 4. The flowchart for generating the p-FE model.

trabecular region in the lower part (“TrabLow”) and trochanter with head. By boolean substraction of cavity and “TrabLow” regions from the entire region we obtain the cortical region. Finally three main solids representing the proximal femur remain: (a) cortical, (b) TrabLow, (c) trochanter and head—see Fig. 3. This separation allows assigning different material properties to each region as will be described in Section 2.2.1. The resulting 3D solid was imported into a p-FE solver and a mesh was generated by an auto-mesher using tetrahedral elements (denoted as “tetra-model”), as well as manually using hexahedral elements (denoted as “hexa-model”). The elements exactly follow the surfaces of the bone. The schematic flowchart that describes the FE generation from CT scans is provided in Fig. 4.

2.2.1. Material properties assignment to the FE model

Isotropic linear elastic properties were considered with inhomogeneous Young’s modulus E being a continuous spatial function independent of the mesh as described in Yosibash et al. (2007) and a constant Poisson’s ratio. Isotropic linear elasticity has been widely used in past FE studies on the proximal femur (Keyak et al., 1990; Lotz et al., 1991a; Cody et al., 1999; Mertz et al., 1996; Taddei et al., 2006), supported by works such as Peng et al. (2006) that reports on small differences in the mechanical response of the femur if the bone is assumed to be either isotropic or anisotropic.

Determination of $E(x, y, z)$ follows the following steps (technical details are described in Yosibash et al., 2007). First a moving average algorithm is applied to average the HU data in each voxel based on a predefined cubic volume of $3 \times 3 \times 3\,\mathrm{mm}^3$ surrounding it (cubic volumes of $2\,764,343\,\mathrm{mm}^3$ showed similar results in Yosibash et al., 2007). HU averaged data were subsequently converted to an equivalent mineral density ρ_{EQM}. The connection (ρ_{EQM}) is determined by the calibration phantom, i.e. five burettes containing different concentrations of K_2HPO_4 ranging from 0 to $300\,\mathrm{mg/cm}^3$—see for details Cann (1988), Yosibash et al. (2007). During CT scans, the phantom was placed as close as possible to the bone to minimize errors introduced by non-uniformity of the CT numbers within the scan filed. An excellent linear correlation between HUs and corresponding concentrations of K_2HPO_4 was established, see Fig. 5:

$$\rho_{\mathrm{EQM}} = 0.0006822 \times \mathrm{HU} - 0.00548\,\mathrm{g/cm}^3, \quad R^2 = 0.998. \tag{1}$$

Next the LMS algorithm was applied to the discrete values of ρ_{EQM}, providing a continuous spatial polynomial approximation

$$\rho_{\mathrm{EQM}} = \sum_{k=0}^{3} z^k \left(\sum_{i,j=0}^{3} a_{ijk} r^i \sin(j\theta) + \sum_{i,j=0}^{3} a_{ijk} r^i \cos(j\theta) \right)$$

in each of the three bone regions, with $R^2 = 0.955-0.977$. Because Young’s modulus is reported as a function of ash density ρ_{ash} or apparent density ρ_{app}, the following connections are required:

$$\rho_{\mathrm{ash}} = 1.22\rho_{\mathrm{EQM}} + 0.0523\,\mathrm{g/cm}^3 \quad \text{see Keyak and Falkinstein (2003),} \tag{2}$$

$$\rho_{\mathrm{app}} = 0.001\mathrm{HU}\,\mathrm{g/cm}^3 \quad \text{see Cody et al. (2000).} \tag{3}$$

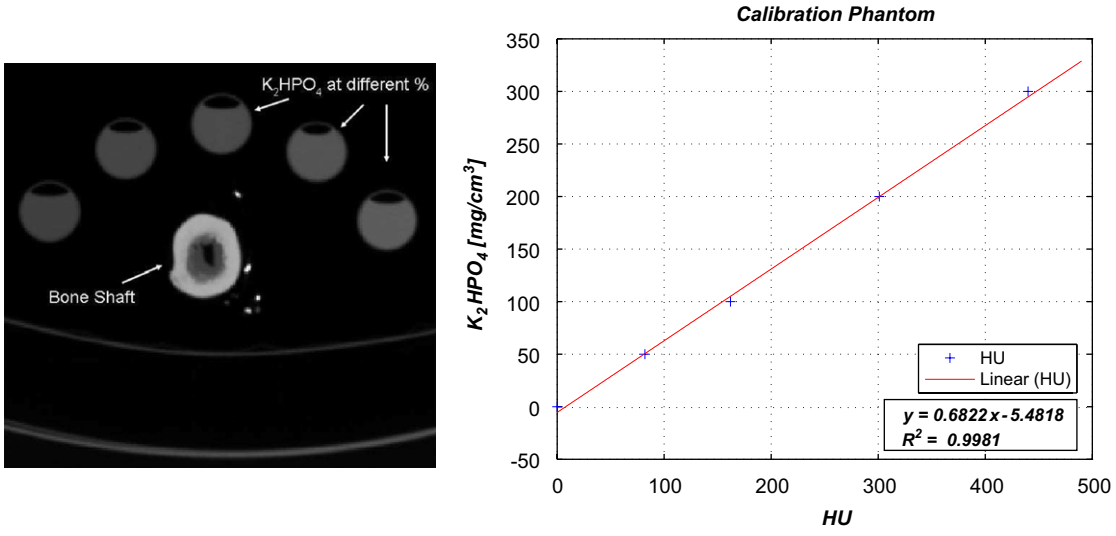

Fig. 5. Estimation ρ_{EQM}(HU) relationship. Left: Scan of bone’s shaft and K_2HPO_4 phantoms; right: ρ_{EQM} and corresponding HU.

Table 1
Summary of $E(\rho)$ relations

Conn. name	No.	$E(\rho)$ relationship	Ref.
Carter and Linde[a]	(c.C&L)	$E_{\mathrm{Cort}} = 2875\rho_{\mathrm{app}}^3$	Carter and Hayes (1977)
	(t.C&L)	$E_{\mathrm{Trab}} = 2003\rho_{\mathrm{app}}^{1.56}$	Linde et al. (1991)
Cody et al.	(c.Co)	$E_{\mathrm{Cort}} = 1684\rho_{\mathrm{app}}^{3.3}$	Cody et al. (2000)
	(t.Co)	$E_{\mathrm{Trab}} = 1949\rho_{\mathrm{app}}^{2.5}$	Cody et al. (2000)
Keyak and Falkinstein	(c.Key)	$E_{\mathrm{Cort}} = 10200\rho_{\mathrm{ash}}^{2.01}$	Keyak and Falkinstein (2003)
	(t.Key)	$E_{\mathrm{Trab}} = 5307\rho_{\mathrm{ash}} + 469$	Keyak and Falkinstein (2003)
Keller	(tc.Kel)	$E = 10500\rho_{\mathrm{ash}}^{2.3}$	Keller (1994)

E in MPa and ρ in g/cm^3.
[a]The combined connections are suggested in San Antonio et al. (2005).

Finally the inhomogeneous Young's modulus is obtained by its relation to ρ_{ash} or ρ_{app} according to Table 1. Notice the differences in respect to Yosibash et al. (2007): herein ρ_{EQM} is the dependent parameter based on which E is determined, and three of the four relationships in Table 1 are different. The different E(HU) relations are shown in Fig. 6. Constant Poisson ratio ν was assigned to the entire bone. According to a sensitivity analysis in Yosibash et al. (2007) and as will be reevaluated herein, the influence of ν on the results is very small. Although linear elastic response of the bone is a widely accepted assumption, supported by many in vitro experiments with a second-order viscoelastic response, the bone is definitely not an isotropic material but rather anisotropic or transversely isotropic in the cortical part. The difficulty in determining the inhomogeneous principle directions and the five required material parameters that determine Hooke's law preclude at this time a more accurate FE analysis.

2.2.2. Boundary conditions and sensitivity tests

Because in Yosibash et al. (2007) we noticed that FE results as sensitive to load boundary conditions, in the present investigation two loading configurations were applied in the experiment and therefore modeled in the FE analysis, see Fig. 7: (a) a pressure on a planar face that trimmed femur's head at $h = 155.5$ and 154.5 mm, (b) tractions on a circular surface determined by the interface of the cone and femur's head. In both cases the head was free to move perpendicular to the load. To ensure the reliability of the FE analyses sensitivity studies were performed: (a) several constant Poisson ratios $\nu = 0.01, 0.1, 0.3, 0.4$ were applied to the entire bone model, as in Cody et al. (2000), Taddei et al. (2006), Yosibash et al. (2007); (b) the distal face residing in PMMA was either clamped or modeled as attached to a distributed spring; (c) strains at SGs locations were obtained in $\pm 5^\circ$ offset orientations; (d) strains were obtained either as averaged over an element or as maximum or minimum values.

3. Results

3.1. In vitro experiments

In all experiments a linear response between force and displacements was observed beyond 200 N preload. Statistical analysis on SGs data shows linear response to load and good repeatability in the entire measurement range.

Displacement rates in the range of 0.1–10 mm/min were applied resulting in similar mechanical response, ensuring that rate of 0.5 mm/min used in the experiments indeed produces a quasi-static response. Linear displacement/load ($\Delta z/\Delta F$ and $\Delta y/\Delta F$) and strain/load ($\Delta\varepsilon/\Delta F$) ratios were computed for each loading and summarized in Table 2. n represents the number of experiments for which data is available. The ratios are computed using linear regression based on the linear response range only (between 200 N to maximum load). Malfunction was observed during the experiments in SG8 resulting in large experimental errors, and in SG2 for the 0°, which were therefore discarded from

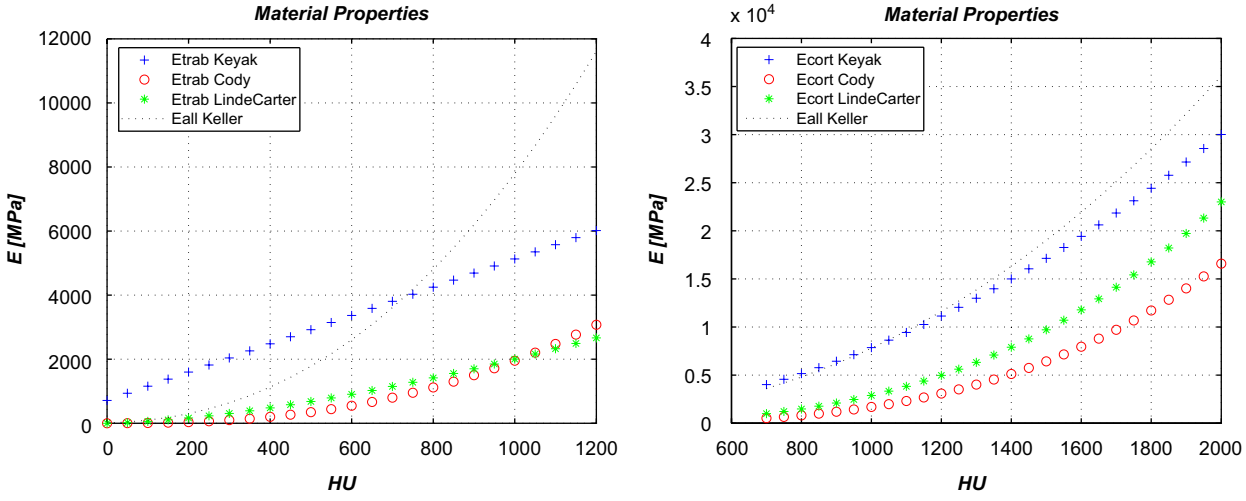

Fig. 6. E(HU) relations according to Table 1.

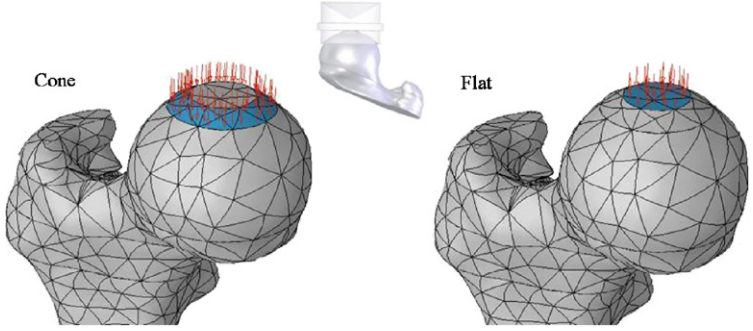

Fig. 7. Load configurations applied at an angle of 0° to the shaft axis.

Table 2
In vitro experiments: head displacement/force (μm/N) measured by LVDTs and strain/force (μstrain/N) SGs measurements

Angle (deg)	n	Mean	Min	Max	Δ (%)	n	Mean	Min	Max	Δ (%)
	$\Delta u_z/\Delta F$ (μm/N)					$\Delta u_y/\Delta F$ (μm/N)				
0	9	0.0004	0.00035	0.00046	13.7	8	0.00066	0.00046	0.0008	25.8
7	6	0.000272	0.00026	0.00029	5.5	5	0.00052	0.00047	0.0006	12.5
20	5	0.0000625	0.00006	0.000065	4	–	N/A	N/A	N/A	N/A
	SG1 (μstrain/N)					SG2 (μstrain/N)				
0	13	0.6565	0.5747	0.7260	11.5	9	−0.0381	−0.0552	−0.02856	−34.9
7	13	0.6200	0.6059	0.6279	1.8	6	−0.3657	−0.3769	−0.3483	−3.9
20	5	−0.0982	−0.1086	−0.0909	−9	5	−0.2764	−0.2941	−0.2655	−5.2
	SG3 (μstrain/N)					SG4 (μstrain/N)				
0	9	−1.1606	−1.2143	−1.0972	−5	13	0.6529	0.5979	0.6975	7.6
7	6	−1.0789	−1.08	−1.0766	−0.2	13	0.5904	0.5867	0.5952	0.7
20	5	−0.5627	−01.5728	−0.548	−2.2	5	0.1982	0.1869	0.2057	4.5
	SG5 (μstrain/N)					SG6 (μstrain/N)				
0	13	−1.3382	−1.3662	−1.3042	−2.3	9	−0.5773	−0.5876	−0.5695	−1.6
7	13	−1.4020	−1.4252	−1.3856	−1.4	6	−0.703	−0.72	−0.6919	−2
20	5	−1.1556	−1.1639	−1.1413	−1	5	−0.609	−0.6168	−0.6014	−1.3
	SG7 (μstrain/N)					SG8 (μstrain/N)				
0	9	0.3752	0.36377	0.38283	2.5	9	0.0907	0.0704	0.1086	21
7	6	0.3537	0.3478	0.36154	1.9	6	0.0675	0.0581	0.0855	20
20	5	0.2395	0.2337	0.2437	2.1	–	N/A	N/A	N/A	N/A

Δ (%) $= 100 * (\max - \min)/(2 \times \text{mean})$.

further analysis. Relatively large experimental errors may be noticed when inspecting the lateral displacement measurement also. The viscoelastic effect was checked by measuring the change in u_z displacement needed to keep a constant 1000 N load during 60 and 120 s at 0° and 7° inclination. A small change of 5%/min in displacement was observed for the cone loaded test and 10%/min change was observed for the flat surface loaded test. Similar behavior was also reported in Keyak et al. (1993), Yosibash et al. (2007).

Finally, loading the bone by a flat surface resulted in slightly different strains and z-displacement compared to the conical device. For the 0° inclination angle the difference was about 3% in strains and 11% in displacement, and for the 7° inclination angle about 8% in strains and 12% in displacement.

3.2. FE verification and sensitivity analysis

The discretization error inherent in the FE model was investigated by comparing the two different FE models, the "hexa model" and the "tetra model", and by increasing the polynomial degree of the shape functions from 1 to 6 in the two models. The Young modulus is the spatial function according to (t.Key) and (c.Key) because these relations produce the closest results compared to the experiments (details in Section 3.3). The tetra/hexa models had about 3000/1000 elements with $\approx 327,000/125,000$ DOFs at $p = 6$, respectively. The estimated relative error in energy norm at $p = 6$ for the "tetra model" is less than 2%, and the strains at the SG location and head displacement are

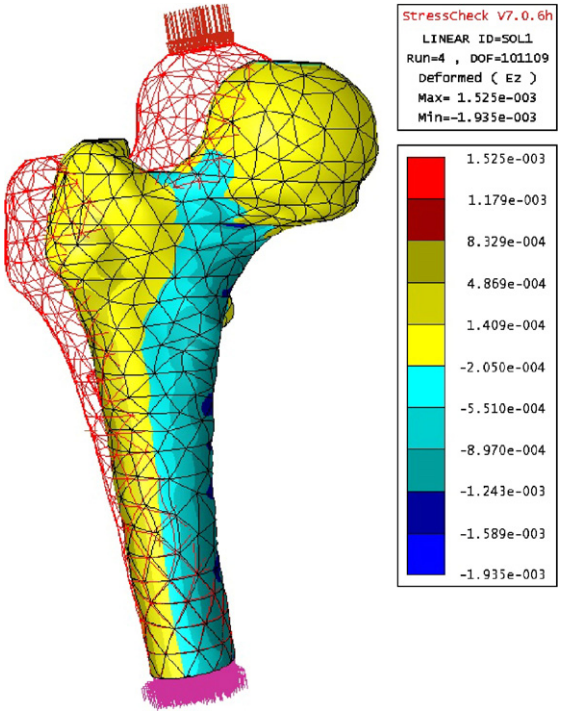

Fig. 8. ε_{zz} for a 1000 N load in the bone at 0° inclination angle.

virtually converged beyond $p = 4$. For the "hexa model" the estimated relative error at $p = 6$ was less than 5%. The extracted strains at the SG location differ in the two models by ~5% and the displacements by less than 1%; therefore the "tetra model" generated by the auto-mesher was used in our subsequent analyses.

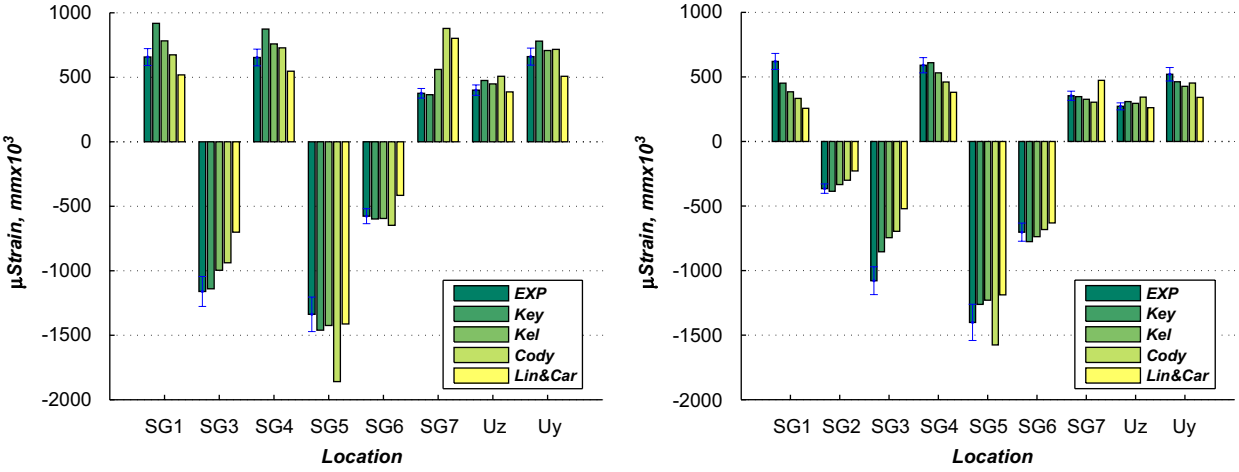

Fig. 9. p-FE compared to experimental observations using the different $E(\rho)$ relationships: load of 1000 N at 0° (left) and 7° (right) inclination angles.

Table 3
Displacements and strains at 1000 N load computed by p-FEs and averaged experimental measurement

Angle (deg)	u_z (mm)			u_y (mm)			SG1 (µstrain)			SG3 (µstrain)		
	FEA	Exp.	Δ (%)	FEA	Exp.	Δ (%)	FEA	Exp.	Δ (%)	FEA	Exp.	Δ (%)
0	0.47	0.4	19	0.78	0.66	18	918	657	40	−1140	−1161	−2
7	0.31	0.27	13	0.46	0.52	−11	450	620	−27	−855	−1079	−21
20	0.073	0.062	17	0.19	N/A	N/A	−373	−98	279	−248	−563	−56
	SG4 (µstrain)			SG5 (µstrain)			SG6 (µstrain)			SG7 (µstrain)		
0	873	653	34	−1461	−1338	9	−598	−557	4	364	375	−3
7	609	590	3	−1262	−1402	−10	−776	−703	10	347	354	−2
20	103	198	−48	−961	−1156	−17	−661	−609	9	325	240	36

Δ (%) = 100 * (FEA−Exp.)/Exp.

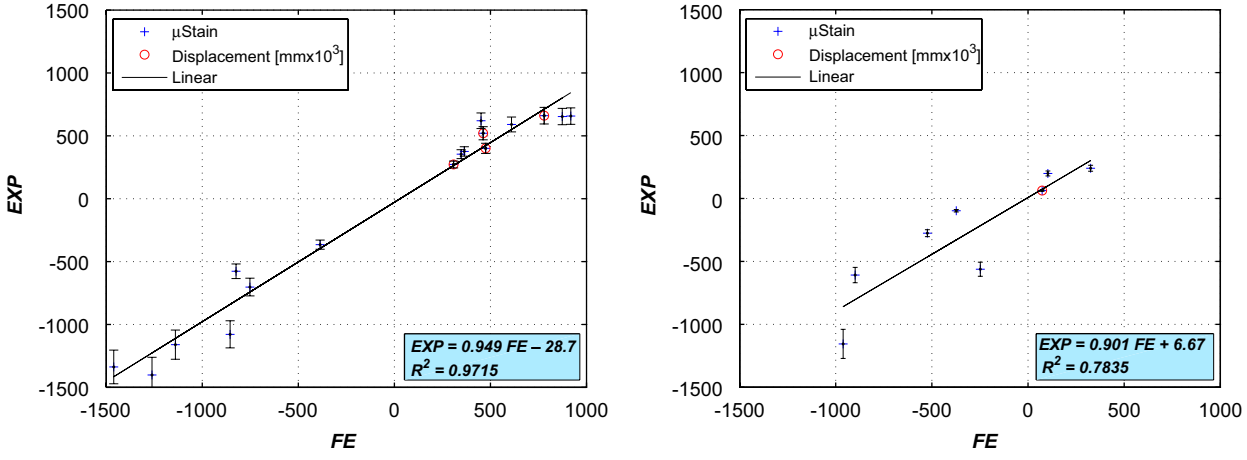

Fig. 10. Linear regression of predicted vs. measured displacement and strains for the 1000 N load: 0° and 7° inclination angle (left) and 20° inclination angle (right).

Negligible influence of v on displacements or strains was observed when assigned to it $v = 0.01, 0.1, 0.3, 0.4$ (changes of less than 5% in strains and less than 1% in displacements). Therefore, $v = 0.3$ (as in many other studies) was used in all subsequent FE analyses. Only SG7 showed a sensitivity of about 30% in the range of $v = 0.01-0.4$.

The loading configurations in Fig. 7 were applied to the 0° and 7° FE models. These two different loading configurations produced differences in the strains of about 3−10% and in the displacements of about 10−14%. The height of the trimmed planar face on which the load is applied ($z = 155.5$ or 154.5 mm) had a minor influence on the result.

The spring boundary conditions at the distal face resulted in virtually identical results as clamped boundary conditions when the spring coefficients were taken high to represent the PMMA and steel stiffness. A representative strain field on the deflected bone is provided in Fig. 8 in which we show ε_{zz} for the 0° inclination at 1000 N load.

3.3. FE validation by experimental observation

The accuracy of the geometry representation of the bone was examined by measuring the outer dimensions of the proximal femur at six locations along its length (using a caliber). The measured dimensions were compared to the FE model resulting in a mean error of 3% (0.91 mm) with a maximum error of 9% (2.38 mm) at the head region (model's dimensions are in most cases smaller than the actual bone).

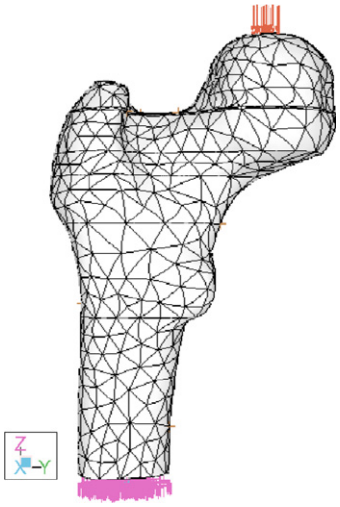

Fig. 11. FE model and BCs of the proximal femur reported in Yosibash 1et al. (2007).

Next the influence of the different relationships $E(\rho)$ in Table 1 was examined by comparing the tetra-mesh results (at $p = 6$ with $v = 0.3$) to the experimental observations for each inclination angle under a load of 1000 N. For example, Fig. 9 shows the comparison (strains and displacements) for 0° and 7° experiments. The E(HU) relation by Keyak and Falkeinstein, (c.Key)–(t.Key), provided the closest results compared to the experimental observations, a trend observed for all inclination angles. This relation is therefore used in the next reported studies. Accurate predictions were obtained for 0° and 7°, whereas for 20° some discrepancy exists. FE strains and displacements compared to these measured in the experiment are summarized in Table 3. Reported FE strains are averaged over the finite element's face because these are correlated to SG readings that are also an average value over SGs length. The predicted strains and displacements correlated well with experimental values for both the 0° and 7° tests (Fig. 10, left). The slope of the regression line is 0.95 (very close to one) and the linear regression coefficient $R^2 = 0.97$ (the intercept is in percentage close to zero). For the 20° test (Fig. 10, right) the correlation is somewhat weaker, with the slope of the regression line 0.9 and $R^2 = 0.78$, and interception close to zero. These results are considered to be in excellent agreement compared to similar reported results as in Keyak et al. (1993), Lotz et al. (1991a), Taddei et al. (2007).

3.4. Revisited analysis of fresh-frozen bone in Yosibash et al. (2007)

The methods described herein were applied to the QCT scans of the fresh-frozen bone loaded by 1500 N force at 0° tilt angle described in Yosibash et al. (2007). The generated FE mesh consists of about 4500 tetrahedral elements resulting in ~300,000 DOF at $p = 5$. Distal face was fully constrained and head planar face was loaded in the z-direction by a 1500 N load and free to move in the

Table 4
SGs and vertical displacements at 1500 N for 0° inclination angle in the past experiment and p-FEA in Yosibash et al. (2007) compared to results obtained by the new methods presented herein

Location	Experiment	Yosibash et al. (2007)	New methods	Δ (%) Yosibash et al. (2007)	Δ (%) New method
SG1 (μStrain)	−1955	−359	−1893	−82	−3
SG2 (μStrain)	660	168	1187	−75	80
SG3 (μStrain)	−1954	−1874	−1878	−4	−4
SG4 (μStrain)	662	1058	617	60	−7
u_z (mm × 10^3)	450	350	528	−22	17

Δ (%) = 100 ∗ (FEA−Exp.)/Exp.

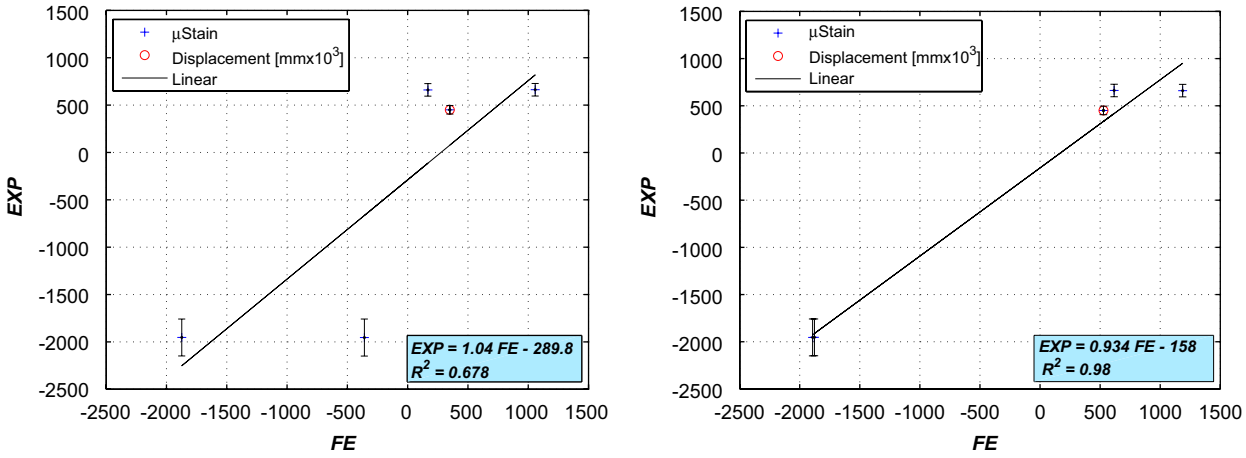

Fig. 12. Linear regression of predicted vs. measured displacement and strains for the bone discussed in Yosibash et al. (2007) at 0° inclination and load of 1500 N using the methods in Yosibash et al. (2007) (left) and the new methods mentioned herein (right).

transverse directions—see Fig. 11. Material properties were assigned according to (t.Key)–(c.Key). Table 4 summarizes the experimental observations and FE results reported in Yosibash et al. (2007), as well as the FE results obtained by the methods described herein, and Fig. 12 compares the linear regression of predicted vs. measured displacement and strains using the methods in Yosibash et al. (2007) and the new methods described herein. The results indicate that the new methods improve significantly the agreement with the experiment data, both when examining the interception point and R^2 that increase from 0.69 to 0.98 (slope of regression line is both cases is close to 1).

4. Discussion

Patient-specific bone FE models generated from QCT data have become of interest because of their high potential in clinic practice. Although automatic mesh generators may provide good and fast geometrical representation of bones, the determination of their cortical/trabecular subdomains and associated material properties is still one of the major difficulty in making these FE models reliable enough for clinical applications. Leveraging on our previous study Yosibash et al. (2007), we enhanced and improved the FE generation and the inhomogeneous Young's modulus determination to reduce idealization errors (introduced by assumptions made to describe a physical system by mathematical models) so to obtain realistic FE models from QCT data. The unique advantage of p-FE methods, allowing us to keep the discretization errors under control, enabled us to focus our attention on the idealization errors. To estimate these, a fresh-frozen human bone was used for in vitro experiments under a variety of boundary conditions. We investigated several E(HU) connections, concluding that the distinct relations in the cortical and trabecular regions (t.Key–c.Key) proposed by Keyak and Falkinstein (2003) (obtained by empirical investigations in the references therein) produce the best correlation to experimental observations. Keller's E(HU) connection (tc.Kel), although not distinguishing between cortical and trabecular bone, results in good predictions, close (but inferior) the ones obtained by using (t.Key–c.Key). Excellent results for both displacements and strains were obtained which correspond very well to the in vitro experimental observations. Although in Yosibash et al. (2007) we concluded that E(HU) connections (t.Co–c.Co) in Cody et al. (2000) are most appropriate for displacement predictions, poor results were obtained for the strain prediction and (t.Key–c.Key) connections were not investigated therein. The revised analysis herein of the data in Yosibash et al. (2007) by the new methods results in considerably better estimation of strains and displacements. If we compare our results (validated on two different in vitro experiments on proximal femurs) with those recently published, see e.g. Keyak et al. (1993), Taddei et al. (2007), Yosibash et al. (2007), we find that our correlation herein is significantly better, with R^2 in the range of 0.95.

The better correlation obtained between FE results and experimental observations for the 0°–7° inclination angle, compared to the 20° inclination angle, may be contributed to the anisotropic material properties (especially in the head region) that have a more pronounced effect for the later case. This will be further investigated in future works.

To further substantiate the reliability of the FE model we performed several sensitivity studies, some which are rarely discussed in other publications. One of these studies is the sensitivity to load application—both the location and method of application, reported in Yosibash et al. (2007) to have a major influence on the results. For the bone model described herein minor change is observed in the FE results if the trimmed planar face on which the load is applied changes by about 1 mm ($z = 155.5$ or 154.5 mm). The configuration of load application was checked both in the FE model and in the experimental protocol by applying the load through a flat surface or conical interface, showing small influence on the results. In the FE analysis in

Yosibash et al. (2007) the plane on which the load was applied was constrained from inplane movement and head geometry was not smoothen—these are the reasons for the large sensitivity reported therein.

Limitations of the present work are: (a) methods have been validated on two normal femur in vitro experiments only, (b) FE model did not take into account the known local anisotropic behavior of the bone tissue. These limitations do not reduce the importance and generality of the obtained results for the following basic reasons. Firstly, a large number of tests were performed (compared to other studies) and many different loading scenarios were considered, hence a large amount of experimental data were available for comparison. Secondly, SGs were placed on the proximal part of the femur, which represents a valid example of a difficult anatomical region to mesh. Regarding the anisotropic behavior, the bone is usually remodeled such that for the experiment configuration (similar to stance posture) the material principal directions are oriented according to principal strains, thus uniaxial properties may be satisfactory. Furthermore, thanks to possible estimation of transversely isotropic material properties (Lotz et al., 1991b; Wirtz et al., 2000; Shahar et al., 2007), a preliminary FE analysis was performed with transversely isotropic material properties assigned to cortical bone (70% of the longitudinal Young's modulus applied in the transverse directions) showing only a slight improvement in the results compared to the experimental observation.

It is important to note that a part of the discarded femur's shaft was also QCT scanned and used thereafter for determination of material properties by methods in Shahar et al. (2007). The Young modulus determined by speckle interferometry was lower by about 20% compared to the E(HU) estimated value using any of the relationships in Table 1. This observation necessitates further investigation into the methods used for the material properties correlation to HUs via density. In this respect, it is important to mention that the trabecular bone in the FE model is divided into two regions, in each different functions representing E(HU) is used. The estimation of these functions is based on points which are slightly outside the region. At the interface of these regions there is a slight jump in the material properties, and results close to the interface may not be very accurate, however, none of the SGs are very close to this interface, so that interface's influence on the results should be minor.

To conclude, semi-automatic procedures for the construction of patient-specific p-FE models (from QCT scans) with distinct trabecular and cortical sub-domains and inhomogeneous Young's moduli are shown to provide very accurate results. Both displacements and strains are predicted in the same range of accuracy as the experimental errors, significantly better than any of the previous publications known to the authors. The entire simulation process requires a couple of hours, including model verification and results inspection (and can be shortened significantly to less than an hour by introducing further automatic procedures), making it suitable for clinical routinely application.

Conflict of interest

None of the authors have any conflict of interest to declare that could bias the presented work.

Acknowledgements

The authors thank Dr. Ron Shahar of the Koret school of veterinary medicine, Hebrew University of Jerusalem for his assistance in bone material property estimation, Mr. Ilan Gilad of Ben-Gurion university for his assistance with the in vitro experiments and generation of the hexahedral mesh, and Dr. Ori Gilad of Tel-Aviv university for his assistance with the Matlab smoothing algorithm.

References

Alho, A., Husby, T., Hoiseth, A., 1988. Bone mineral content and mechanical strength. An ex-vivo study on human femora and autopsy. Clinical Orthopaedics 227, 292–297.

Bayraktar, H., Morgan, E., Nieber, G.L., Morris, G., Wong, E., Keaveny, M., 2004. Comparison of the elastic and yield properties of human femoral trabecular and cortical bone tissue. Journal of Biomechanics 37, 27–35.

Bessho, M., Ohnishi, I., Matsuyama, J., Matsumoto, T., Imai, K., Nakamura, K., 2007. Prediction of strength and strain of the proximal femur by a CT-based finite element method. Journal of Biomechanics 40 (8), 1745–1753.

Cann, C., 1988. Quantitative CT for determination of bone mineral density: a review. Radiology 166, 509–522.

Carter, D., Hayes, W., 1977. The compressive behavior of bone as a two-phase porous structure. Journal of Bone and Joint Surgery—American Volume 59, 954–962.

Cody, D., Gross, G., Hou, F., Spencer, H., Goldstein, S., Fyhrie, D., 1999. Femoral strength is better predicted by finite element models than QCT and DXA. Journal of Biomechanics 32, 1013–1020.

Cody, D., Hou, F.J., Divine, G.W., Fyhrie, D.P., 2000. Short term in vivo study of proximal femoral finite element modeling. Annals Biomedical Engineering 28, 408–414.

Couteau, B., Payan, Y., Lavallee, S., 2000. The mesh-matching algorithm: an automatic 3d mesh generator for finite element structures. Journal of Biomechanics 33, 1005–1009.

Cowin, S., Ashby, M., 2001. Bone Mechanics Handbook. CRC Press, Boca Raton.

Esses, S., Lotz, J., Hayes, W., 1989. Biomechanical properties of the proximal femur determined in vitro by single-energy quantitative computed tomography. Journal of Bone and Mineral Research 4, 715–722.

Heismann, B., Leppert, J., Stierstorfer, K., 2003. Density and atomic number measurements with spectral X-ray attenuation method. Journal of Applied Physics 94, 2073–2079.

Jensen, J., 1978. A photoelastic study of a model of the proximal femur. A biomechanical study of unstable trochanteric fractures I. Acta Orthopaedica Scandinavica 49 (1), 54–59.

Keaveny, T., Guo, E., Wachtel, E., McMahon, T., Hayes, W., 1994. Trabecular bone exhibits fully linear elastic behavior and yields at low strains. Journal of Biomechanics 27, 1127–1136.

Keller, T., 1994. Predicting the compressive mechanical behavior of bone. Journal of Biomechanics 27, 1159–1168.

Kenney, J., Keeping, E., 1962. Mathematics of Statistics. Van Nostrand, Princeton, NJ.

Keyak, J., Falkinstein, Y., 2003. Comparison of in situ and in vitro CT scan-based finite element model predictions of proximal femoral fracture load. Medical Engineering and Physics 25, 781–787.

Keyak, J., Fourkas, M., Meagher, J., Skinner, H., 1993. Validation of automated method of three-dimensional finite element modelling of bone. ASME Journal of Biomechanical Engineering 15, 505–509.

Keyak, J., Meagher, J., Skinner, H., Mote, J., 1990. Automated three-dimensional finite element modelling of bone: a new method. ASME Journal of Biomechanical Engineering 12, 389–397.

Linde, F., Norgaard, P., Hvid, I., Odgaard, A., Soballe, K., 1991. Mechanical properties of trabecular bone: dependency on strain rate. Journal of Biomechanics 24 (9), 803–809.

Lotz, J., Gerhart, T., Hayes, W., 1990. Mechanical properties of trabecular bone from the proximal femur: a quantitative CT study. Journal of Computer Assisted Tomography 14 (1), 107–114.

Lotz, J., Cheal, E., Hayes, W., 1991a. Fracture prediction for the proximal femur using finite element models: Part 1— linear analysis. ASME Journal of Biomechanical Engineering 113, 353–360.

Lotz, J., Gerhart, T., Hayes, W., 1991b. Mechanical properties of metaphyseal bone in the proximal femur. Journal of Biomechanics 24, 317–329.

Mertz, B., Niederer, P., Muller, R., Ruegsegger, P., 1996. Automated finite element analysis of excised human femura based on precision-QCT. ASME Journal of Biomechanical Engineering 118, 387–390.

Peng, L., Bai, J., Zeng, Z., Zhou, Y., 2006. Comparison of isotropic and orthotropic material property assignments on femoral finite element models under two loading conditions. Medical Engineering and Physics 28, 227–233.

San Antonio, T., Araque, E., Casanova, E., Muller-Karger, C.M., 2005. Sensitivity analysis of heterogeneous mechanical properties of a bone model. In: Rodrigues, H.e.a. (Ed.), Proceedings of ICCB05— III International conference on computational bioengineering (Lisbon, Portugal), vol. 1. IST press, pp. 209–220.

Shahar, R., Zaslansky, P., Barak, M., Friesem, A., Currey, J., Weiner, S., 2007. Anisotropic Poisson's ratio and compression modulus of cortical bone determined by speckle interferometry. Journal of Biomechanics 40, 252–264.

Szabó, B.A., Babuška, I., 1991. Finite Element Analysis. Wiley, New York.

Taddei, F., Pancanti, A., Viceconti, M., 2004. An improved method for the automatic mapping of computed tomography numbers onto finite element models. Medical Engineering and Physics 26, 61–69.

Taddei, F., Cristofolini, L., Martelli, S., Gill, H., Viceconti, M., 2006. Subject-specific finite element models of long bones: an in vitro evaluation of the overall accuracy. Journal of Biomechanics 39, 2457–2467.

Taddei, F., Schileo, E., Helgason, B., Cristofolini, L., Viceconti, M., 2007. The material mapping strategy influences the accuracy of CT-based finite element models of bones: an evaluation against experimental measurements. Medical Engineering and Physics 29 (9), 973–979.

Viceconti, M., Bellingeri, L., Cristofolini, L., Toni, A., 1998. A comparative study on different methods of automatic mesh generation of human femurs. Medical Engineering and Physics 20, 1–10.

Viceconti, M., Davinelli, M., Taddei, F., Cappello, A., 2004. Automatic generation of accurate subject-specific bone finite element models to be used in clinical studies. Journal of Biomechanics 37, 1597–1605.

Wirtz, D., Schiffers, N., Pandorf, T., Radermacher, K., Weichert, D., Forst, R., 2000. Critical evaluation of known bone material properties to realize anisotropic FE-simulation of the proximal femur. Journal of Biomechanics 33, 1325–1330.

Yosibash, Z., Padan, R., Joscowicz, L., Milgrom, C., 2007. A CT-based high-order finite element analysis of the human proximal femur compared to in-vitro experiments. ASME Journal of Biomechanical Engineering 129 (3), 297–309.